Enhancing Isolation in Solidly Mounted Resonators for Brain Implantable Microbots

Laura Mazón Maldonado, Mahdieh Shojaei Baghini, Roghaieh Parvizi, Hadi Heidari

Microelectronics Lab (meLAB), James Watt School of Engineering, University of Glasgow, G12 8QQ, UK
l.mazon-maldonado.1@research.gla.ac.uk and Hadi.Heidari@glasgow.ac.uk

***Abstract*— Implantable brain devices have been used for deep brain neurostimulation over past decades. Wireless power and data transmission is still one of the main challenges in such devices. Among various technologies for providing high performance power/data rate, microfabricated magnetoelectric resonators such as Solidly Mounted Resonators (SMR), are often utilized in microwave applications due to their high tolerance and electromechanical coupling. In this study, we propose the optimization of a multilayer SMR to be implemented in brain microbots. The Multiphysics simulations are carried out via finite element modeling in COMSOL. ZnO was used as active layer of the SMR, and its thickness was tuned to obtain peak resonance at 2.5 GHz, with a layer of SiO_2 as encapsulant. The shift in the resonant frequency with varying number of stacks beneath the active area was analyzed, finding first sharp the fundamental mode of resonance around 1.3 GHz on average. Based on our simulation results, SMRs with a quality factor up to 963 were designed, with an improved S_{11} of -15.15 dB.**

Keywords—SMR, resonator, piezoelectric, reflector, scattering parameter, Bragg reflector.

I. INTRODUCTION

Implantable neural interfacing devices struggle with the brain tissue reaction to traditional implantation designs [1]. The device activation method and the transmission of power and data are key factors to enable their operation for neurostimulation and recording. There are multiple techniques for power and data transmissions such as inductive and capacitive coupling, magnetic resonant coupling and mid/far-field antennas [2]. These last ones will be our subject of study.

For that reason, the research about RF acoustic resonators that uses the coupling of magnetoelectric and piezoelectric materials is essential. This kind of resonators enable the actuation of the implantable microbots via magnetic field, as well as a wireless transmission of power and data, causing minimal tissue damage and offering a considerable improvement to brain implantable devices [1], [3]–[5].

Radio frequency piezoelectric resonators are becoming of great interest in implantable microbots due to their high scalability. These devices generate a time-varying electric field via the application of a harmonic stress [6]. This facilitates their use for a variety of applications such as communication devices, chemical vapour sensors and energy harvesting.

Bulk Acoustic Wave (BAW) resonators have gained traction due their ability to be aggressively miniaturized and their frequency tuning capabilities. They can also operate at ultra-high frequencies, extending up to 20 GHz and beyond, in contrast to the performance of Surface Acoustic Wave (SAW) resonators, which exhibit decaying efficiency beyond 2 GHz [7]. Despite the presence of a high-quality factor (Q-factor) in BAWs resonators, degradation in device performance is observed due to energy losses. The main loss factor at BAWs is caused by the contact between the piezoelectric material and the substrate. To reduce the wave propagation between them, the main structures that have been proposed are FBARs (thin-film bulk acoustic wave resonators) and SMRs (solidly mounted resonators) [7], [8].

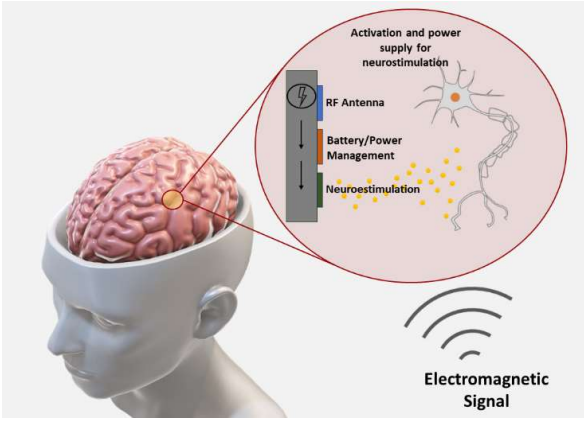

Figure 1. Schematic figure of the use of a SMR as power source and antenna in a microbot for neurostimulation. The application of this implant is to treat diseases such as Alzheimer.

SMRs are devices that make use of Bragg reflectors to acoustically isolate the piezoelectric film from the substrate. They consist of alternating low acoustic impedance and high acoustic impedance materials. The highest the ratio high impedance-low impedance, the highest the reflection is [9]. The fabrication of SMRs is simplified due to the absence of air gaps. Due to their semi-planar structure, they can be encapsulated with biocompatible materials such as Silica and Parylene-C aiding in their use as implants. That is why we carry out in this paper a study of the Bragg reflector for the reflection of longitudinal waves, as early research to develop nanomechanical magnetoelectric antennas for autonomous microbots in the European project CROSSBRAIN as visualised in Fig. 1 [10]. The aim of this project is to develop microbot technology to stimulate brain tissue selectively for the treatment of pathological brain conditions, such as Alzheimer. In this paper, the design of the SMR is highlighted in Section II. The simulation methodology, results and conclusions are presented in Section III, Section IV, and Section V, respectively.

Funded by EU's HORIZON-EIC-2021-PATHFINDERCHALLENGES - GA n. 101070908.

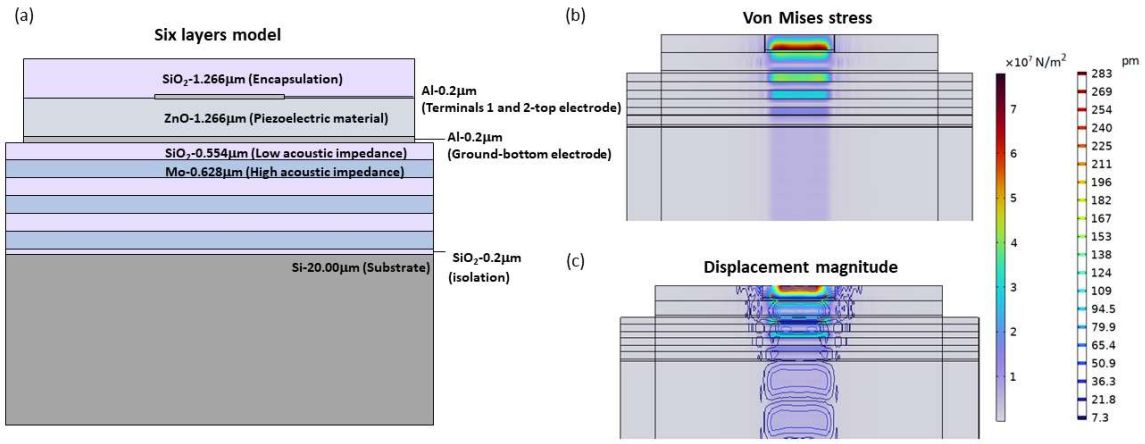

Figure 2. Design of the BAW resonator used for Study A with a six-layer Bragg reflector (a). Distribution of the stress along the active area of the resonator for its fundamental resonant mode (b). Results for its surface displacement at 1.34 GHz using Contour in COMSOL multiphysics (c).

II. DEVICE DESIGN

The resonator consists of ZnO as the piezoelectric layer and alternating stacks of Silica and Mo in the DBR (distributed Bragg reflector). The aforementioned have been chosen due to their acoustic actuation capabilities as well as complementary metal oxide semiconductor (CMOS) compatibility. We based our design on the work of Yujin Li *et al.* [11], adapting it to a resonant frequency of 2.5 GHz for ZnO under a layer of SiO_2 layer as an encapsulation.

TABLE I

THICKNESS OF THE CONSTITUTING LAYERS OBTAINED USING EQ. 1.

Material	υ (m/s)	Thickness (µm)
ZnO	6330	1.266
SiO_2	2170	0.554
Mo	6280	0.628

The resonant frequency of the resonator is determined primarily by the thickness of the piezoelectric layer, which is λ/2, given by Eq. 1.

$$t = \lambda/(2n) = \upsilon/(2\,f_0) \quad (1)$$

Where t is the thickness of the layer, λ is the wavelength, n is the refraction index of the material, υ is the acoustic velocity of the material and f_0 the resonant frequency. Following a study of the Fresnel reflections utilised to determine the layer thicknesses as given by Eq.1, to obtain a maximized reflection of longitudinal waves, the thickness of the layers in the Bragg reflector must be λ/4. The materials used for the stack are SiO_2, as our low acoustic impedance material, and Mo, as the high acoustic impedance material. The number of pairs required in the stack is determined by the high to low acoustic impedance ratio. In this case the ratio is 5, which translates to six layers within the stack [12].

To study the performance of the Bragg reflector, two different studies were carried out:

- **Study A:** DBRs with an even number of layers (2,4,6,8 and 10).
- **Study B:** DBRs with an odd number of layers (3,5,7, 9 and 11 layers). For which we added a SiO_2 layer beneath the stacks in Study A.

The six-layers model employed in Study A is shown in Fig. 2(a). It consists of an encapsulating layer, a top electrode, a piezoelectric layer, a bottom electrode, a Bragg reflector and a substrate top to bottom. This structure was repeated for every model.

III. METHODOLOGY

These studies were carried out in COMSOL Multiphysics, starting from the Thin-Film BAW resonator model available in their library. Our programs make use of three studies explained below. The first study uses the solid mechanics module to obtain the eigenfrequencies of the resonant modes. A peak voltage of 1V is applied across the piezoelectric material, which produces a mechanical strain in the film via the inverse piezoelectric effect. This is given by Eq. 2, taking into account the electrical behaviour of the material and Hook's law.

$$\boldsymbol{S} = \boldsymbol{sT} + d^t\boldsymbol{E} \quad (2)$$

$\boldsymbol{S}$ is the strain, $\boldsymbol{s}$ the compliance in short-circuit conditions, $\boldsymbol{T}$ is the stress and $\boldsymbol{d}$ is the piezoelectric tensor.

The second study analyses the frequency response to the application of 1V. That way, we obtain the short circuit input admittance (Y_{11}). For the third study, however, we replace the terminal voltage of the top electrode with an input power of 0.1W (Terminal 2 in Fig. 2(a)) to extract the quality factor (Q-factor) and the scattering parameter (S_{11}) of each model.

To characterize our models, we also estimated the values of the Figure of Merit (FOM) and the coupling coefficient (K_{eff}^2) for each model. They are defined in Eq. 3 and Eq 4.

$$FOM = {k_{eff}}^2 Q \quad (3)$$

$${k_{eff}}^2 = \frac{\pi^2}{4}\frac{f_a - f_r}{f_a} \quad (4)$$

where f_a is the frequency of antiresonance and f_r the resonant frequency.

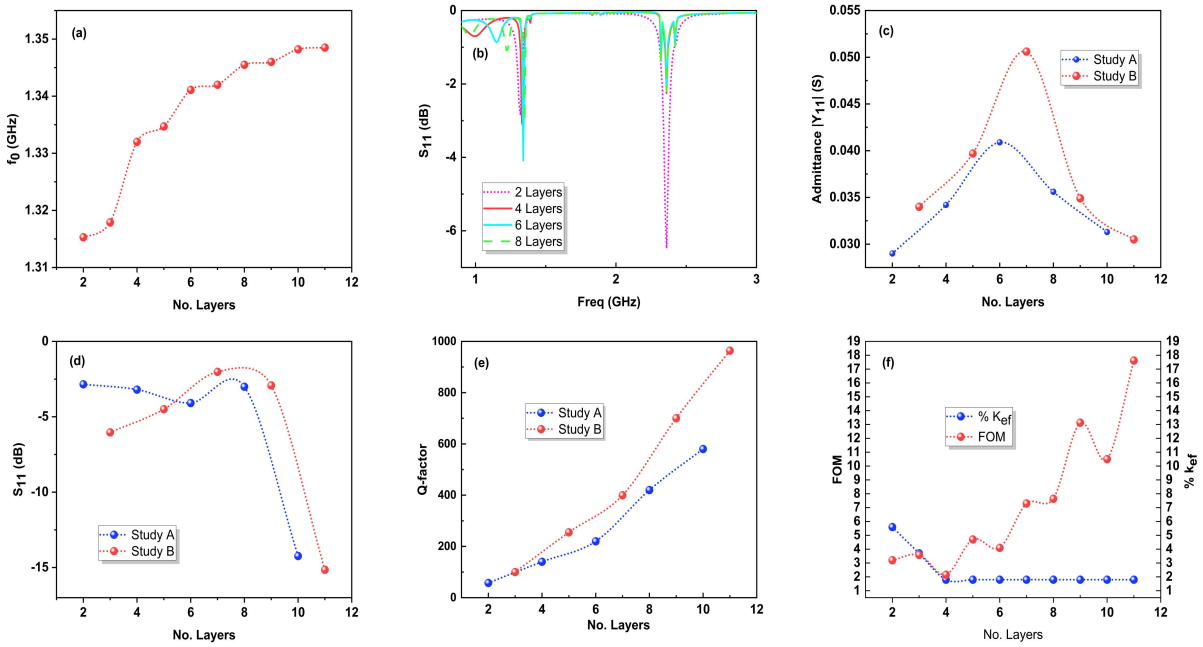

Figure 3. Progression of the resonant frequency shift of the fundamental mode from 2.5 GHz for each model (a). Dependence of the scattering parameter S_{11} with the frequency for the Study A models (b). Admittance at the fundamental resonant mode for each of the simulated models (c). Measurements of the S_{11} parameter at the fundamental resonant mode for each of the simulated models (d). Quality factor measured at the eigenfrequency of the fundamental mode of resonance for the models of Studies A and B (e). Figure of Merit (FOM) and coupling coefficient (k_{ef}) in percentage for each model (f).

IV. Results and Discussion

Fig. 2(b) shows how the inverse piezoelectric effect takes place in the resonator, as a result of the internal electric field. The distribution of the von Mises stress is located mainly in the vicinity of the electrodes. The peak stress of magnitude $7\times10^7 N/m^2$ lies above the top electrode, within the encapsulating layer. This strain corresponds to surface displacements, in the range of 10^{-6}µm in Fig. 2(c). The resonant frequency varies considerably with the loss in the system, where we have acoustic losses, ohmic losses of the electrodes and laterally leaking waves, making it challenging to develop an accurate resonator for a specific frequency [11]. The frequency response study captured this shift of the fundamental mode of resonance. We can clearly see in Fig. 3(a) how this frequency increases with the number of layers that is present in the device, changing from 1.315 GHz for the two-layer stack to 1.349 GHz for the eleven-layer one. The drop in the resonance frequency is shown in Fig. 3(a) shift. This reduction is less pronounced when we add a SiO_2 (density of 2170 kg/m^3) layer at the bottom of the stack as compared to when Mo is added (density of 10200 kg/m^3).

The parameter S_{11} or return loss, measures how much power is reflected in the device [13]. In Fig. 3(b) we can see this shift of the peaks for the scattering parameter S_{11}. Their position moves to higher frequencies for their fundamental mode with increasing layers. It also shows how, even though we designed our devices to reach resonance at 2.5 GHz, the maximum values are shifted to lower frequencies close to 2.4 GHz.

The admittance of the models experiences a clear growth for the reflectors with a low number of layers. The maximum values are 0.041 S for Study A and 0.051 S for Study B, as Fig. 3(c) shows. Nonetheless, when the number of layers at the stack increases above 7, the admittance lowers, which could take place because of the increasing number of discontinuities in the impedance at the reflector.

Fig. 3(d) represents the scattering parameter values that each device reaches for studies A and B. We can appreciate how for an even number of layers (Study A) the performance of the stack improves when adding more pairs of them in general. It experienced a progress from -2.85 dB for a two-layers stack to -14.24 dB for the ten-layers one. However, for Study B we can see that increasing the number of layers did not improve the reflection of the waves for the first three reflectors. Nevertheless, when we reach the nine-layers stack, the radiation of the resonator starts growing, giving the best isolation for the resonator with an eleven-layers stack with -15.15 dB.

Table II

Q-factor values found for different SMRs designs.

No. of layers	Freq. (GHz)	Materials	Q factor	Reference
1	2.3	SiO_2	150	[14]
Multi-layer (unknown)	2.3	-	67	[14]
11	3.5	SiO_2/Ta_2O_5	165	[15]
5	2.46	SiO_2/Mo	250	[16]
11	2.5	SiO_2/Mo	963	Present work

Overall, adding layers immediately after the recommended number of layers of the stack with the ratio high-acoustic-impedance/low acoustic impedance, did not

make and improvement in the radiation of the signal. On the other hand, the Q factor measures the damping of the resonators. Following the study of S. Jose *et al*. [7], the losses are minimized when the number of layers is odd. In Fig. 3(e) we can see that the damping of the resonance is reduced by increasing the number of layers at the Bragg reflector in both studies. However, the results are better for some models of the Study B, even if there are less layers in their stack than in the Study A ones: The five-layer resonator has a Q-factor of 255 while the six-layers one is 224. Furthermore, we found the best result for the eleven-layers resonator instead of the ten-layer one, with a Q-factor of 963.

In Fig. 3(f) we can see how the FOM grows, in general, with the addition of layers at the stack, even though the coupling coefficient (K_{eff}^2) does not show any change by using more than four of them. In the literature we could find similar studies that showed some good quality factors. H. P. Löbl *et al*. [14] conducted a study of resonators operating between 0.9 and 2.3 GHz for a one-layer acoustic reflector. They obtained a quality factor of 130-150, and for a multi-layer λ/4 reflector it was between 18 and 67. Closer to our designs, Lu Lv *et al*. used an eleven λ/4 layers stack with a Q-factor of 165 at 3.5 GHz [15]. These values, already considered adequate for the isolation from the substrate, are far from the results that belong to our models, already mentioned. This comparison of our higher Q-factor value with similar published works can be found in Table II.

V. Conclussion and future work

We carried out a complete study of the reflection of the longitudinal waves along a resonator using different designs for a Solidly Mounted Resonator. The effect of the damping of the materials was easily appreciated by the shift of the fundamental mode resonant frequency, that was found at approximately 1.3 GHz. The results obtained for the S_{11} parameter point out that the radiation of the resonators enhances by adding layers to the reflector in general. The values out of the tendency may be caused by scattering of the waves when combining a certain number of impedance discontinuities. We obtained high quality factors for λ/4 Bragg reflectors. These values experimented an increase when we added a low acoustic impedance layer (SiO_2) at the bottom of the stack, improving the stability of the resonance of the device. We found the highest value for an eleven-layers stack, with a Q-factor of 963, a value considerably above of the results found in the literature for this type of design. Therefore, we can conclude that the damping of the resonant behaviour of the piezoelectric material lowers by adding λ/4 layers in a Bragg reflector, improving it when the number of them is odd. As future work, we will fabricate nanomechanical magnetoelectric antennas, coupling the piezoelectric layer with a magnetostrictive material, making use of a high number of layers Bragg reflector.

Ackwledgement

This work was supported by the European CROSSBRAIN project, funded by the European Union's European Innovation Council, call HORIZON-EIC-2021-PATHFINDERCHALLENGES-01-02, under Grant Agreement n. 101070908.

References

[1] E. McGlynn, R. Das, and H. Heidari, "Encapsulated magnetoelectric composites for wirelessly powered brain implantable devices," in *ICECS 2020 - 27th IEEE International Conference on Electronics, Circuits and Systems, Proceedings*, 2020. doi: 10.1109/ICECS49266.2020.9294847.

[2] J. Zhang, R. Das, J. Zhao, N. Mirzai, J. Mercer, and H. Heidari, "Battery-Free and Wireless Technologies for Cardiovascular Implantable Medical Devices," *Advanced Materials Technologies*, vol. 7, no. 6. 2022. doi: 10.1002/admt.202101086.

[3] R. Das, F. Moradi, and H. Heidari, "Biointegrated and Wirelessly Powered Implantable Brain Devices: A Review," *IEEE Transactions on Biomedical Circuits and Systems*, vol. 14, no. 2. 2020. doi: 10.1109/TBCAS.2020.2966920.

[4] F. Walton, E. McGlynn, R. Das, H. Zhong, H. Heidari, and P. Degenaar, "Magneto-Optogenetic Deep-Brain Multimodal Neurostimulation," *Advanced Intelligent Systems*, vol. 4, no. 3, 2022, doi: 10.1002/aisy.202100082.

[5] E. McGlynn *et al.*, "The Future of Neuroscience: Flexible and Wireless Implantable Neural Electronics," *Advanced Science*, vol. 8, no. 10. 2021. doi: 10.1002/advs.202002693.

[6] K. M. Lakin, "A review of thin-film resonator technology," *IEEE Microw Mag*, vol. 4, no. 4 SPEC. ISS., 2003, doi: 10.1109/MMW.2003.1266067.

[7] S. Jose, A. B. M. Jansman, and R. J. E. Hueting, "A design procedure for an acoustic mirror providing dual reflection of longitudinal and shear waves in Solidly Mounted BAW Resonators (SMRs)," in *Proceedings - IEEE Ultrasonics Symposium*, 2009. doi: 10.1109/ULTSYM.2009.5442065.

[8] R. Thalhammer and R. Aigner, "Energy loss mechanisms in SMR-type BAW devices," in IEEE MTT-S International Microwave Symposium Digest, 2005. doi: 10.1109/MWSYM.2005.1516565.

[9] F. Z. Bi and B. P. Barber, "Bulk acoustic wave RF technology," *IEEE Microw Mag*, vol. 9, no. 5, 2008, doi: 10.1109/MMM.2008.927633.

[10] "Crossbrain", https://crossbrain.eu/ (Accessed: 15 July 2023).

[11] Y. Li, X. Yuan, and W. Zou, "Simulation and analysis of thin film bulk ultrasonic transducers and optimization acousto-optical coupling," in Nanophotonics, Nanoelectronics and Nanosensor, N3 2013, 2013. doi: 10.1364/n3.2013.nsa3a.16.

[12] F. H. Villa-López, G. Rughoobur, S. Thomas, A. J. Flewitt, M. Cole, and J. W. Gardner, "Design and modelling of solidly mounted resonators for low-cost particle sensing," *Meas Sci Technol*, vol. 27, no. 2, 2015, doi: 10.1088/0957-0233/27/2/025101.

[13] H. Ja'afar, M. T. B. Ali, A. N. B. Dagang, H. M. Zali, and N. A. Halili, "A Reconfigurable Monopole Antenna with Fluorescent Tubes Using Plasma Windowing Concepts for 4.9-GHz Application," *IEEE Transactions on Plasma Science*, vol. 43, no. 3, 2015, doi: 10.1109/TPS.2015.2398878.

[14] H. P. Löbl *et al.*, "Materials for bulk acoustic wave (BAW) resonators and filters," *J Eur Ceram Soc*, vol. 21, no. 15, 2001, doi: 10.1016/S0955-2219(01)00329-6.

[15] L. Lv et al., "BAW Resonator with an Optimized SiO2/Ta2O5Reflector for 5G Applications," ACS Omega, vol. 7, no. 24, 2022, doi: 10.1021/acsomega.2c01749.

[16] E. Lugo-Hernández et al., "Analysis of spurious peaks at series resonance in solidly mounted resonators by combined BVD-Mason modelling," Ultrasonics, vol. 131, p. 106958, 2023. doi:10.1016/j.ultras.2023.106958